Mechanical Properties, Structure, Bioactivity and Cytotoxicity of Bioactive Na-Ca-Si-P-O-(N) Glasses

Assia Mabrouk, Ahmed Bachar, Ali Atbir, Claudine Follet-Houttemane, Cyrille Albert-Mercier, Arnaud Tricoteaux, Anne Leriche, Stuart Hampshire

Mechanical properties, structure, bioactivity and cytotoxicity of bioactive Na-Ca-Si-PO-(N) glasses

Assia Mabrouk, Ahmed Bachar, Ali Atbir, Claudine Follet, Cyrille Mercier, Arnaud Tricoteaux, Anne Leriche, STUART HAMPSHIRE

Mechanical Properties, Structure, Bioactivity and Cytotoxicity of Bioactive Na-Ca-Si-P-O-(N) Glasses

Assia Mabrouk, Ahmed Bachar, Ali Atbir, Claudine Follet, Cyrille Mercier, Arnaud Tricoteaux, Anne Leriche, Stuart Hampshire

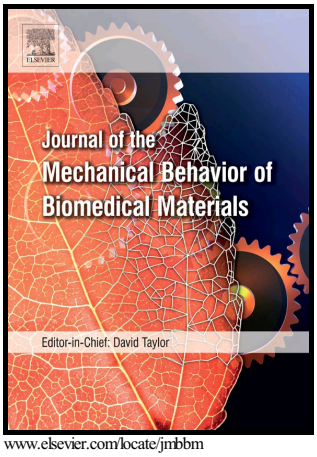

www.elsevier.com/locate/jmbbm

PII: S1751-6161(18)30419-3
DOI: https://doi.org/10.1016/j.jmbbm.2018.06.023
Reference: JMBBM2844

To appear in: *Journal of the Mechanical Behavior of Biomedical Materials*

Received date: 28 March 2018
Revised date: 14 May 2018
Accepted date: 18 June 2018

Cite this article as: Assia Mabrouk, Ahmed Bachar, Ali Atbir, Claudine Follet, Cyrille Mercier, Arnaud Tricoteaux, Anne Leriche and Stuart Hampshire, Mechanical Properties, Structure, Bioactivity and Cytotoxicity of Bioactive Na-Ca-Si-P-O-(N) Glasses, *Journal of the Mechanical Behavior of Biomedical Materials,* https://doi.org/10.1016/j.jmbbm.2018.06.023

Mechanical Properties, Structure, Bioactivity and Cytotoxicity of Bioactive Na-Ca-Si-P-O-(N) Glasses

Assia Mabrouk[a], Ahmed Bachar[b,c], Ali Atbir[c], Claudine Follet[d], Cyrille Mercier[d], Arnaud Tricoteaux[d], Anne Leriche[d], Stuart Hampshire[e*] .

[a]CEMHTI CNRS UPR3079, 1D Av. de la recherche scientifique, 45071 Orléans Cedex 2, France.

[b]Campus Universitaire-Ait Melloul, Université Ibn Zohr, Agadir, Morocco.

[c]LGP, Chemical Department, Faculty of Sciences, Université Ibn Zohr, B.P. 8106, Agadir, Morocco.

[d]Univ. Valenciennes, EA 2443 – LMCPA – Laboratoire des Matériaux Céramiques et Procédés Associés, F-59313, Valenciennes, France.

[e]Materials and Surface Sciences, Bernal Institute, University of Limerick, Limerick, Ireland.

assia.mabrouk@cnrs-orleans.fr

a.bachar@uiz.ac.ma

a.atbir@uiz.ac.ma

Claudine.Follet@univ-valenciennes.fr

cyrille.mercier@univ-valenciennes.fr

Arnaud.Tricoteaux@univ-valenciennes.fr

anne.leriche@univ-valenciennes.fr

stuart.hampshire@ul.ie

[*]**Corresponding author**. Tel:+353(0)61202640, fax: +353(0)61338172.

Abstract

Bioactive glasses are able to bond to bone through formation of carbonated hydroxyapatite in body fluids. However, because of their poor strength their use is restricted to non-load-bearing applications. The effects of nitrogen addition on the physical and mechanical properties and structure of bioactive oxynitride glasses in the system Na–Ca–Si–P–O–N have been studied. Glasses with compositions (mol.%): $29Na_2O–13.5CaO–2.5P_2O_5–(55−3x)SiO_2–xSi_3N_4$ (x is the no. of moles of Si_3N_4) were synthesised with up to 1.5 at.% P and 4.1 at.% N. A novel 3-step process was used for addition of P and N and this proved successful in minimising weight losses and producing homogeneous glasses with such high SiO_2 contents. The substitution of 4.12 at.% N for oxygen results in linear increases in density (1.6%), glass transition temperature (6%), hardness (18%) and Young's modulus (74%). Vickers Indentation Fracture (VIF) resistance (K_{ifr}) was calculated from various relationships depending on the load, indent diagonal, crack lengths and Young's modulus to hardness (E/H) ratio. Firstly, Meyer's index n is calculated from the slope of the logarithmic plot of load versus indent diagonal. Then by comparing the experimental slopes of the logarithmic plots of crack lengths versus load it is concluded that the cracking mode is Radial Median type. The substitution of 4.12 at.% N for oxygen results in an increase in K_{ifr} of 40%. These increases in properties are consistent with the incorporation of N into the glass structure in three-fold coordination with silicon which results in extra cross-linking of the glass network. The structure of these bioactive oxynitride glasses was investigated by solid state nuclear magnetic resonance (MAS NMR) of ^{31}P and ^{29}Si. The structure reveals that all the N atoms are bonded to Si atoms with the formation of SiO_3N, SiO_2N_2 and Q^4 structural units with extra bridging anions at the expense of Q^3 units. The bioactivity of the glasses has been evaluated by soaking them in simulated body fluid (SBF) and results confirm that all these oxynitride glasses are bioactive. Cytotoxicity tests based on different concentrations of these bioactive glass powders in a cell growth environment have also shown that they are not cytotoxic.

Graphical abstract

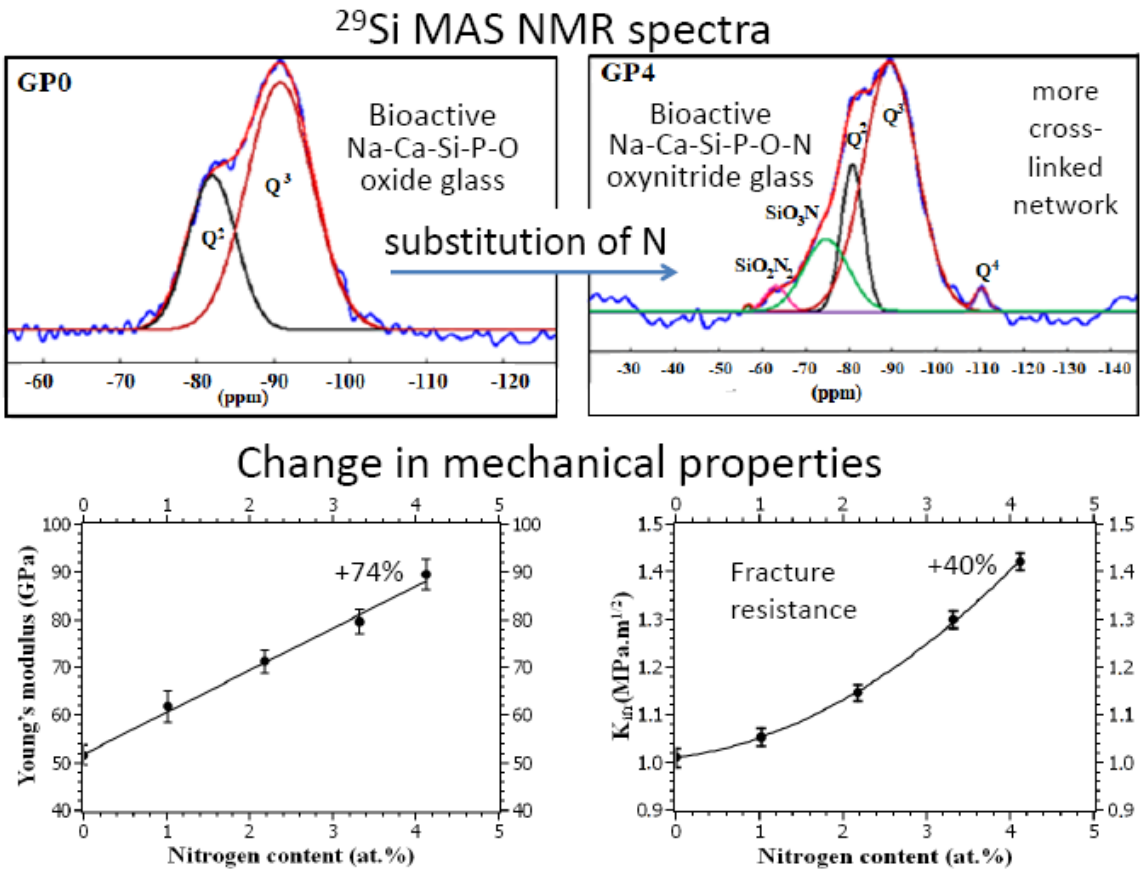

Keywords: Bioactive glass; oxynitride glass; mechanical properties; fracture resistance; thermal properties; glass structure.

1. Introduction

Bioactive glasses are materials able to develop a Hydroxy-Carbonate Apatite layer (HCA) at their surface when soaked in a body fluid [1-3]. The formation of this layer, along with a satisfactory osteoblast interaction, is believed to be an essential condition for bonding to living bone [4,5]. Moreover, HCA allows a stable and durable anchoring to form between an implant and the host environment. Thus, these types of glasses have been developed over the past few decades in order to repair, replace or augment parts of the skeletal system during surgery [1-8].

Hench was the first researcher to prepare a bioactive glass [1,2,4]. His composition, known as Bioglass® 45S5, contains (mol. %): 46.1% SiO_2, 26.9% CaO, 24.4% Na_2O and 2.6% P_2O_5. 45S5 signifies that the glass contains 45 wt.% SiO_2 and has a Ca:P ratio = 5 which is much higher than in the mineral hydroxyapatite found in natural bone, $Ca_5(PO_4)_3OH$ (Ca:P = 1.67).

The higher amounts of Na_2O and CaO, as well as the relatively high CaO/P_2O_5 ratio make the glass surface highly reactive in a physiological environment [1-6]. Hench found that this glass rapidly bonded to bone, did not form any interfacial scar tissue isolating it from the host bone and also stimulated bone growth away from the bone-glass interface [4,5].

Application of Bioglass® 45S5 particles to bone defects results in new bone growth during the first few weeks after surgery [9]. It has been used in more than a million patients to repair bone defects in the jaw and in orthopaedics [6,10]. However, the low mechanical strength and inherent brittleness of bioglasses have restricted their use to non-load-bearing applications such as ossicles in the middle ear [11] and maxillofacial applications including dental bone regeneration [6].

One solution to the challenge of low strength glasses is to incorporate nitrogen into the silicate network [12-14]. When nitrogen replaces oxygen in alumino-silicate glasses, glass transition temperature, elastic modulus and hardness increase linearly with nitrogen content [12-18]. In a study of substitution of N for O in a potentially bioactive glass composition in the SiO_2–CaO–Na_2O system, it was shown that nitrogen increases mechanical properties [14,17] and this can be explained by the fact that N may be viewed as a network forming anion [19].

The aim of the current work was to study the effect of nitrogen on mechanical properties and structure of bioactive glasses in the SiO_2–CaO–Na_2O–P_2O_5 system. Phospho-oxynitride glasses have been prepared in M-P-O-N (where M is a modifier cation) systems. Glass preparation in systems containing Si (and Al) and phosphorus has proved to be difficult due to the fact that oxynitride glasses are melted under slightly reducing conditions in a nitrogen atmosphere such that volatilisation of phosphorus would occur above 800°C [20]. Therefore, synthesis of these bioactive glasses needs to be carefully controlled and depends on several parameters including types of reagents, crucibles, steps used for melting, atmosphere, time and temperature. Thus, a strategy was adopted of using a 3-stage process for melting. Properties of these new Si–Ca–Na–P–O–N glasses were compared with those of glasses in the SiO_2–CaO–Na_2O–P_2O_5 system with the same Na:Ca:Si:P ratios so that any changes are simply a result of changes in O:N ratio. Structural analysis of glasses was characterized using ^{29}Si and ^{31}P MAS NMR spectroscopy. The bioactivity of the glasses has been evaluated by soaking them in simulated body fluid (SBF). The changes at the glass surface as a function of soaking time in the SBF were analyzed by X-ray diffraction (XRD) and SEM combined with EDS. The cytotoxicity has also been studied with the L132 epithelial cell line to assess the

ability of the bioactive glasses for bone reconstruction. Cytotoxicity tests based on different concentrations of glass powders in a cell growth environment have also been evaluated.

2. Experimental Methods

2.1. Glass preparation

Based on previous investigations of glass melting and bioactivity by some of the present authors [21], a base oxide soda-lime-silica glass containing P_2O_5 was chosen with composition (mol.%): $29Na_2O–13.5CaO–2.5P_2O_5–55SiO_2$. Oxynitride glasses were then prepared of molar composition: $29Na_2O–13.5CaO–2.5P_2O_5–(55−3x)SiO_2–xSi_3N_4$ (x is the no. of moles of Si_3N_4) using reagent grade Na_2CO_3 (Merck, purity 99.9%), $CaCO_3$ (Chimie-Plus-Laboratoire, 99%), $(NaPO_3)_n$ (Merck, purity 99.8%), SiO_2 (Merck, pure quartz) and Si_3N_4 (UBE industries, minimum purity 98%, main impurity: oxygen). The weights of reagents were calculated taking into account their purity as shown in Table 1.

Table 1: Weight percentages of oxides/ Si_3N_4 used to prepare Na–Ca–P–Si–O–N glasses

Wt. %	SiO_2	CaO	Na_2O	P_2O_5	Si_3N_4
GP0	40.08	17.34	36.05	6.52	0
GP1	39.38	17.04	35.41	6.42	1.76
GP2	37.30	17.12	35.57	6.45	3.56
GP3	35.19	17.21	35.76	6.49	5.35
GP4	33.07	17.29	35.95	6.52	7.17

The glasses were designed so that constant cation ratios could be maintained independent of nitrogen addition. Thus, the N:O ratio is the only compositional variable which changes and the effects of variations in cation ratio on glass structure and properties are eliminated. Initial experiments resulted in high weight losses and a phosphorus-based solid residue which evolved from the melt. Therefore, as the reaction of P_2O_5 and Si_3N_4 results in loss of P_2 and N_2 [20], base oxide glasses were first prepared without P or N followed by incorporation of nitrogen from Si_3N_4 into the glasses and finally addition of P in the following sequence of steps:

1) Synthesis of base oxide glasses without P_2O_5 with molar proportions: $29Na_2O–13.5CaO–(55−3x)SiO_2$. These were melted in air in platinum crucibles at 1400°C for 2 hours.

2) Preparation of SiO_2–CaO–Na_2O–Si_3N_4 glasses by mixing of the crushed base oxide glass powders with varying amounts (x = 1, 2, 3, 4) of silicon nitride (Si_3N_4) powder. The powders were weighed and mixed in a glass dish using a magnetic stirrer in 50 ml isopropanol and then the alcohol evaporated by heating. Powder batches were pressed under 300 MPa uniaxial pressure and small powder compacts of 1 cm height were obtained.

3) The mixed oxynitride powder compacts were melted in boron nitride lined graphite crucibles in a vertical tube furnace under flowing high purity N_2 at 1350°C for 20 min.

4) The resulting crushed oxynitride glass powders were mixed with the appropriate amount of P_2O_5 using a magnetic stirrer in 50 ml isopropanol and then the alcohol evaporated by heating. Powder batches were pressed under 300 MPa uniaxial pressure and small powder compacts of 1 cm height were obtained.

5) The final compacts, containing all the components, were melted in boron nitride lined graphite crucibles in a vertical tube furnace under flowing high purity N_2 at 1350°C for 20 min.

6) Following melting, glasses were annealed just below the glass transition temperature for 1 hour followed by slow cooling to ambient in order to eliminate stresses that would remain after rapid cooling.

2.2. Glass Characterization

The density was measured using a Helium pycnometer on crushed glasses in order to eliminate the effects of any internal porosity, such as gas bubbles.

Polished samples were examined under a reflected light microscope and then under a scanning electron microscope (Hitachi S4500) coupled with energy dispersive spectroscopy (EDS: Kevex) to analyse the relative Si, Ca, Na, P and O contents. Measurement of N content was carried out using multi-element micro-mapping electron microprobe analyser (Cameca SX 50), along with quantitative wavelength dispersive spectrometry (WDS) to carry out spot chemical analyses at 15 kV, 200 nA. A PC2 Ni/C multi-layer crystal was used to detect Kα X-rays for N. The standard used was BN. For each glass, 10 measurements were performed to ascertain nitrogen homogeneity and to evaluate the average N content in the glasses. The

background noise used in the assessment of the N Kα peak height for the oxynitride glass samples was measured on an oxide glass.

XRD analysis was performed on a D8 Advance Brucker-Brentano diffractometer using Cu $K\alpha_1$ radiation (λ = 1.54056 Å) equipped with a Vantec-1 linear detector, in the 2θ range = 10–120°, in increments of 0.02° and acquisition time of 1 s per step. The ICDD JCPDF database was used for the identification of the crystalline phases.

The glass transition temperature (Tg) of each glass was measured by Differential Scanning Calorimetry (DSC, SETARAM multi-HTC). For each sample, 0.05 g (50mg) of finely ground glass was tightly packed into a platinum crucible to ensure good thermal contact. The sample was heated in argon with a heating rate of 10°C/min up to 1200 °C. Accuracy obtained for Tg determination is ±2 °C.

2.3. Structural Analysis using Nuclear Magnetic Resonance Spectroscopy

The ^{29}Si and ^{31}P MAS NMR experiments were performed on a Bruker Avance I spectrometer operating at 7.0 T, corresponding to ^{29}Si and ^{31}P Larmor frequencies of 59.6 and 121.5 MHz, respectively. The spectrometer was equipped with a 4 mm MAS probe head and the spectra were recorded at a spinning frequency of 14 kHz. ^{29}Si MAS NMR spectra were recorded by accumulating between 1864 and 5120 scans depending on the sample, with pulse duration of 1 μs (corresponding to a flip angle of 18°) and a recycle delay of 60 s. ^{31}P MAS NMR spectra were recorded by accumulating 64 scans with a pulse duration of 0.6 μs (corresponding to flip angle of 15°) and a recycle delay of 30 s. The ^{29}Si and ^{31}P chemical shifts were referenced relative to tetramethylsilane (TMS) and 85% H_3PO_4 solutions, respectively.

2.4. Mechanical Properties

Determination of microhardness and Young's modulus measurements in the present work are as outlined previously by Bachar et al. [22,23]. The fracture resistance of the glasses was assessed using the Vickers indentation test. This method involves pressing a Vickers (diamond) indenter into the glass in order to generate cracks at the extremities of the indent. Then the Vickers Indentation Fracture (*VIF)* resistance is calculated from the dimensions of the indent diagonals and of the crack lengths. This method is particularly useful for rapid evaluation of material properties of small components when sizes of available samples are

limited [24] and therefore has proven useful for assessment of fracture resistance of materials during their development. However, critics of the Vickers indentation test method have characterized it as unreliable for determination of fracture toughness [25]. Nevertheless, using calibration constants that have been empirically determined and adjusted according to the material under investigation, reasonable results can be achieved and, because it is convenient and practically easy to carry out with small sample requirement, the indentation technique has been evaluated more recently [26] as a necessary qualitative tool to determine comparative fracture resistance parameters of different ceramics and glasses. However, as the Vickers Indentation Fracture test is not standard, the calculated value may not be considered equivalent to the fracture toughness, K_{Ic}, of the material. Miyazaki et al. [26] used the term Vickers Indentation Fracture resistance (*VIF* resistance or K_{ifr}) and this approach has been used here. For silica-rich glasses, $K_{ifr}>K_{Ic}$, while for stiffer and harder glasses, such as oxynitride glasses, $K_{Ic}>K_{ifr}$ [27].

In practice, it is generally known that cracks develop following Radial-median or Palmqvist or intermediate modes as represented schematically in Fig.1.

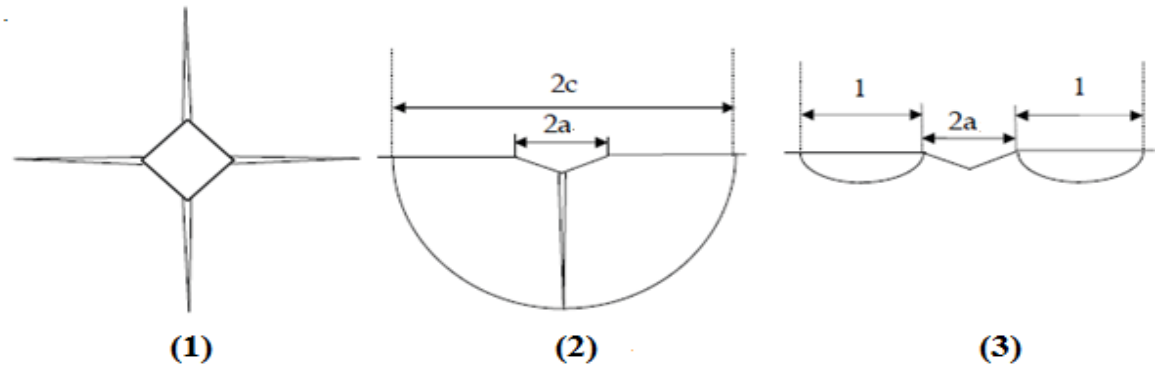

Fig. 1: Schematic of Vickers indentation cracks: (1) appearance of indented surface; (2) cross-sectional view of median/radial cracks; (3) Palmqvist cracks

The *VIF* resistance (K_{ifr}) is calculated from various relationships depending on the load, indent diagonal, crack lengths and Young's modulus to hardness (E/H) ratio. Ponton and Rawlings [28] have reviewed the literature and report approx. twenty equations depending on the cracking mode. More recently, Chicot and Tricoteaux [29] have compared the various equations and proposed average relationships as follows according to the cracking mode:

For Radial-median cracks:

$$K_{ifr(R-M)} = 0.0154(\frac{E}{H_v})^{1/2}\frac{P}{C^{3/2}} \quad (1)$$

For Palmqvist cracks:

$$K_{ifr(P)} = 0.0089(\frac{E}{H_v})^{2/5}\frac{P}{al^{1/2}} \quad (2)$$

For intermediate cracks:

$$K_{ifr(IM)} = (\alpha - \beta q)\times f(\frac{E}{H_v})\frac{P}{a^q c^{(1.5-q)}} \quad (3)$$

where P is load and the parameters a, c and l are defined in Fig. 1. The calculation of the constants α, β, q and of the function *f*(E/Hv) are detailed in a previous report [23].

From a general point of view, K_{ifr} is an intrinsic parameter of a material and consequently it should be independent of applied load. Under these conditions, the different load to crack dimension ratios should be constant. In addition to the direct load-dependence due to P, the ratios involving the half-diagonal of the indent are also connected to the applied load through the Indentation Size Effect (ISE). A simple relationship connecting the half-diagonal, a, to the applied load, P, is given by Meyer [30] as follows:

$$P = Ad^n \quad (4)$$

where A is a constant, d is the indent diagonal equal to 2a and n is known as Meyer's index. If n = 2, then there is no ISE.

From Eq. (4), the half diagonal of the indent, a, is related to the applied load, P, by:

$$a = 0.5\left[\frac{P}{A}\right]^{1/n} \quad (5)$$

When relationship (5) is introduced into equations (1), (2) and (3), the following proportionalities hold:

$c \alpha P^{2/3}$ for relationship (1) - radial-median cracking mode (6)

$1 \alpha P^{2(1-[1/n])}$ for relationship (2) - Palmkvist cracking mode (7)

$c \alpha P^{\left(\frac{1}{(1.5-q)(1-[q/n])}\right)}$ for relationship (3) - Intermediate cracking mode (8)

Consequently, the two crack lengths, c and l, are represented as a function of the applied load, P, in bi-logarithmic coordinates. The experimental slopes are afterwards compared to the theoretical ones depending on Meyer's index, n. In practice, the usual cracking mode can be identified by comparing the experimental slope of ln(c) = f(ln P) to 2/3 for Radial-median cracks or by comparing the experimental slope of ln(l) = f(ln P) to 2/(1−1/n) for Palmqvist cracks. If the experimental slope values do not correspond to the theoretical values, then an intermediate cracking mode may be assumed.

When the experimental slope of ln(c) = f(ln P) is compared with the exponent of relationship (8), then knowing Meyer's index simply allows the determination of the coefficient q and, hence, K_{ifr} using Eq. (3). This last methodology for determining q can be applied to any case by calculating:

$$q = \left[\frac{1.5s - 1}{s - (1/n)} \right] \quad (9)$$

where s is the experimental slope of the plot of ln(c) versus ln P and derives from Eq. (8).

2.5. Bioactivity tests in SBF solution

Glass cylinders of dimensions 15 mm in diameter and 3 mm in height were polished using 2400 grit silicon carbide coated paper. The polished glass pieces were ultrasonically cleaned in an isopropanol bath. *In vitro* bioactivity tests were carried out on the dried glass plates by soaking them in simulated body fluid (SBF) [23] for 15 days. The changes at the glass surface as a function of soaking time in the SBF were analyzed by X-ray diffraction (XRD) and SEM combined with EDS as outlined in ***section 2.2***.

2.6. Cytotoxicity tests

Cytotoxicity tests evaluate the relative plating efficiency (RPE) and subsequently the 50% lethal concentration LC50 (or RPE 50) by means of the colony-forming assay with epithelial cell line (L132 cells) [31]. According to the International and European Standards (ISO10993-5/EN30993-5), the L132 epithelial cell line is selected for its good reproducibility and cloning efficiency (about 37%) [32]. The L132 cells, in minimum essential medium (MEM) supplemented with 10% foetal calf serum (FCS), were continuously exposed to gradually increasing concentrations (0, 25, 50, 100, 200, 400 mg L^{-1}) of glass powder (20 μm diameter

granules) without renewal of the growth environment during the experiments. After a culture period lasting nine days, the environment was removed and the colonies were stained with violet crystal. The number of colonies was then counted under a binocular microscope. At least six repeat experiments were performed, in triplicate for each concentration group. Results are expressed as mean values ± SD with respect to the control (an environment without glass powder, 100%). Pure nickel powder with average particle size of 4-6 μm was also tested as a positive control for comparison.

3. Results and Discussion

3.1. Glass Synthesis and Appearance of Glasses

The experimental strategy of using different steps for addition of P and N proved to be successful in minimising weight losses. Table 2 compares the elemental analyses (in atomic % of the elements) of the initial compositions and the glasses after melting.

At. %	Si		Ca		Na		P		O		N	
	Th.	Exp. ± 0.01	Th.	Exp. ± 0.01	Th.	Exp. ± 0.01	Th.	Exp. ± 0.01	Th.	Exp. ± 0.01	Th.	Exp. ± 0.01
GP0	19.03	19.23	4.67	4.65	20.07	20.01	1.74	1.68	54.49	54.43	0	0
GP1	18.67	18.73	4.58	4.68	19.70	19.80	1.71	1.55	53.99	54.42	1.35	1.02
GP2	18.81	18.92	4.61	4.77	19.84	19.95	1.70	1.54	52.30	52.64	2.74	2.18
GP3	18.93	19.03	4.65	4.95	19.96	20.16	1.72	1.53	50.60	51.01	4.14	3.32
GP4	19.06	19.18	4.67	4.79	20.11	20.22	1.74	1.57	48.88	50.12	5.54	4.12

Th. = Theoretical; Exp. = Experimental

Table 2: Atomic percentages of elements in Na–Ca–P–Si–O–N glasses

Approximately 3% phosphorus was lost when synthesising the oxide glass. The experimental values of both nitrogen and phosphorus contents are lower than the theoretical values for each glass composition, which may be attributed to volatilization of P and N according to [20]:

$$\frac{1}{3}Si_3N_4 + \frac{2}{5}P_2O_5 \rightarrow SiO_2 + \frac{2}{5}P_2 + \frac{2}{3}N_2 \qquad (10)$$

Elemental analysis confirmed that approximately 75% of the initial nitrogen was retained in each composition and >90% P was retained in the oxynitride glasses despite much larger losses expected from equation (10). The difficulties of combining SiO_2, P_2O_5 and N in the same melt to produce glasses has been reported [20] and previously only much smaller amounts of silica could be incorporated when P_2O_5 and N were present. Thus it is remarkable that in the current work homogeneous Na-Ca-Si-O-P-N glasses have been synthesised which retain a substantial amount of the P and N introduced in the initial composition. The overall importance of this work is that while phosphate glasses containing N are well known, to our knowledge this is the first report of successfully prepared glasses containing P and N with such high SiO_2 content (55 mol.%).

The glasses were observed to be transparent but with a grey colour (see Fig. 2).

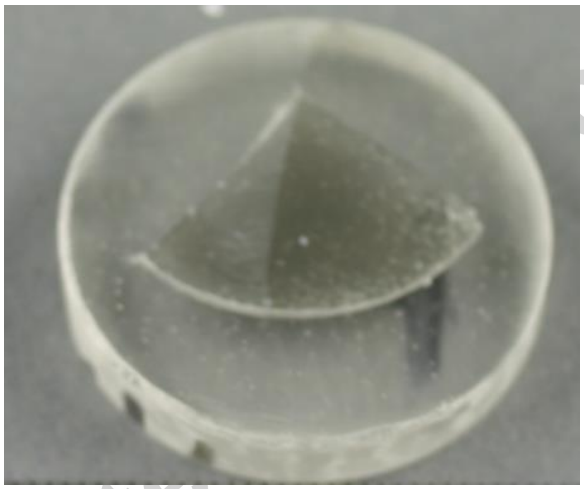

Fig. 2: Typical glass in the Si-Ca-Na-O-P system

X-ray diffraction analysis confirmed that no crystalline phases were present in any of the compositions shown in Table 2, indicating that all glasses are completely amorphous. Cross sections of the glasses were examined by Scanning Electron Microscopy (SEM) to analyze homogeneity and the presence of bubbles. Fig. 3 shows the state of the nitrogen-free GP0 glass and the GP4 glass with maximum nitrogen content. Glasses without N were free of bubbles but all glasses containing N showed evidence of bubbles leaving macroporosity in the glasses. This has implications for the mechanical properties of the glasses.

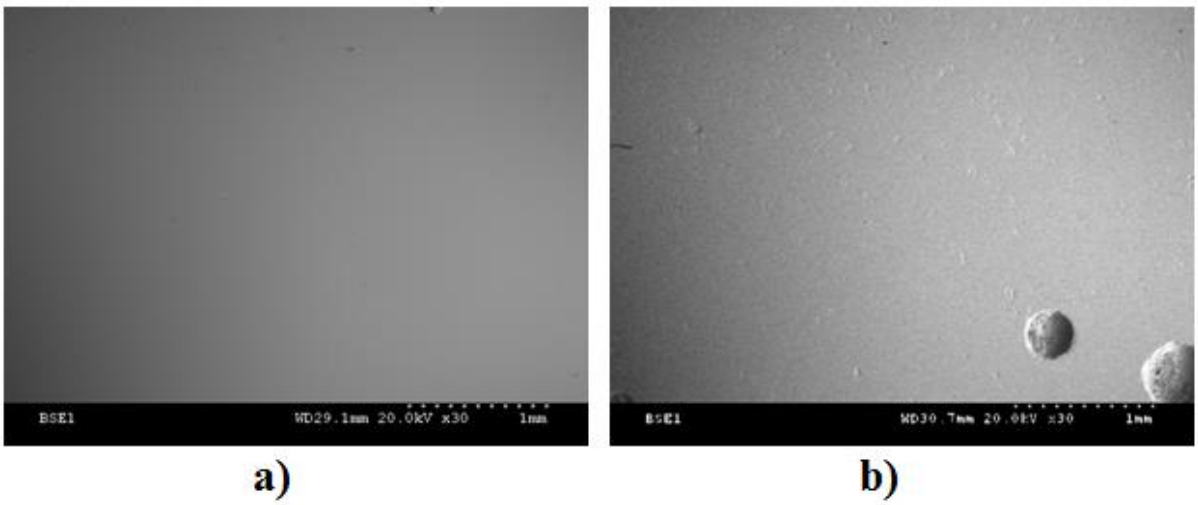

Fig. 3: Low magnification SEM micrographs of cross sections of glasses: a) GP0, b) GP4, showing presence of some bubbles

Despite the presence of bubbles, glass synthesis using the three-step process is successful in producing homogeneous Na–Ca–Si–P–O–N glasses.

3.2. Density and Molar Volume

The effect of nitrogen on the density of the Si–Ca–Na–O–P glasses is shown in Fig. 4 using final analysed nitrogen contents. The variation in density observed with increasing nitrogen is quite significant and increases from 2.50 g/cm^3 for GP0 to 2.54 g/cm^3 for GP4 glass composition. Given that the only compositional variable which changes is N:O ratio, and that tri-coordinated N substitutes for di-coordinated O, then it is clear that, for each % increase in nitrogen content, the same number of extra cross-links are introduced into the glass network [33]. This will have the effect of contracting the network and therefore reducing molar volume and this is consistent with the increase in density with increasing nitrogen content.

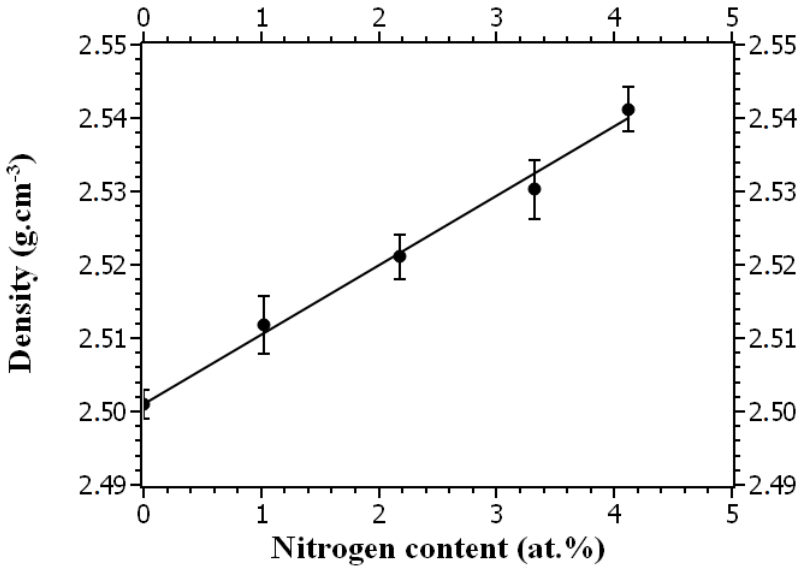

Fig. 4: Density of Na–Ca–P–Si–O–N glasses as a function of nitrogen content

3.3. Glass Transition Temperature Tg

Fig. 5 shows glass transition temperature, determined from DTA experiments, as a function of analysed nitrogen content and, as can be seen, there is a fairly linear increase in glass transition temperature, Tg, from 558°C at 0 at.% N to 581°C at 4.12 at.% N (4% increase). The increase in Tg with N is consistent with previous studies of oxynitride glasses [12-18] which have shown that N creates extra cross-linkages and stiffens the glass network [33].

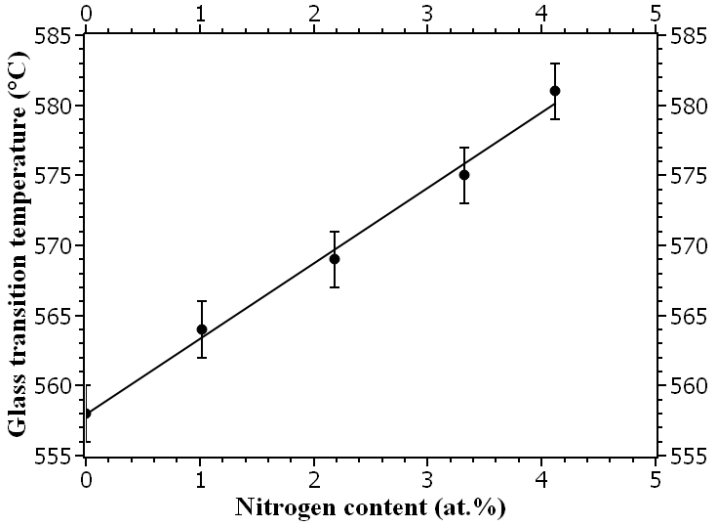

Fig. 5: Glass transition temperature (Tg) of Na–Ca–P–Si–O–N glasses as a function of N content.

3.4. Mechanical properties

3.4.1 Vickers Microhardness and Elastic Modulus

The Vickers microhardness (Hv) as a function of N content for the glasses is shown in Fig. 6. Microhardness increases fairly linearly with nitrogen content as reported previously for oxynitride glasses [10-14] from 4.80±0.04 GPa for 0 at.% N to 5.86±0.07 GPa (18% increase) at 4.12 at.% N.

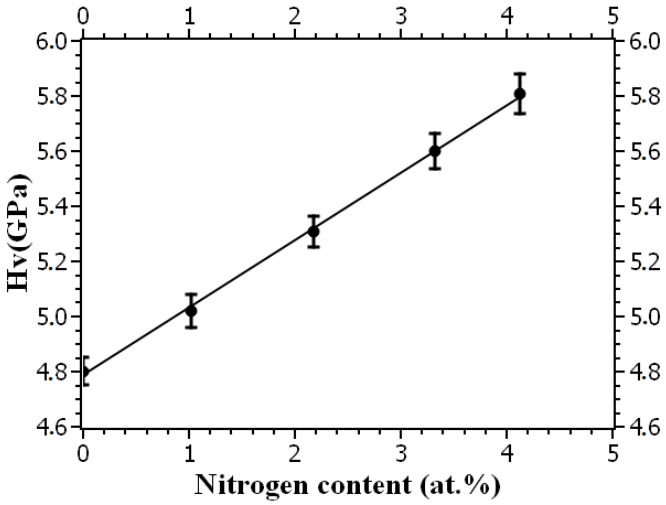

Fig. 6: Vickers microhardness of Na–Ca–P–Si–O–N glasses as a function of nitrogen content

Fig. 7 shows Young's modulus (E) as a function of N content for the glasses and, as can be seen, E increases almost linearly from 51±3 GPa for 0 at.% N to 89±5 GPa (74% increase) at 4.12 at.% N. Increases in E with N are consistent with results of other studies of oxynitride glasses [14,17,33].

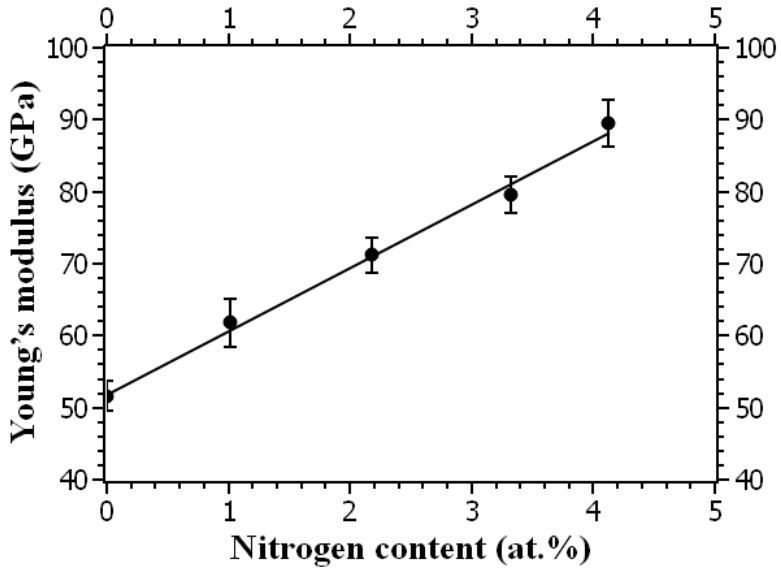

Fig. 7: Young's modulus of Na–Ca–P–Si–O–N glasses as a function of nitrogen content

When comparing these results with those reported earlier for oxynitride and oxyfluoronitride glasses [17,23], it can be seen from the empirical relationships that the slopes of plots of Hv versus N for these new N-substituted Na-Ca-P-Si glasses and for the previous oxyfluoronitride glasses are identical (~0.30 GPa/at.% N). For oxynitride glasses (without fluorine), the slope is somewhat lower but this was thought to be due to the presence of bubbles in the glass. The benefit of nitrogen seems to be similar for the glasses studied here and bioactive glasses containing nitrogen which have been previously reported [14,17,18,22,23].

3.4.2. Vickers Indentation Fracture (VIF) Resistance

For evaluation of VIF resistance, ten Vickers indentations at eight loads ranging from 150 g to 500 g were carried out on the five glasses. Dimensions of indent diagonals and cracks lengths were measured on optical micrographs and using the image analysis software ImageJ©.

The first step in the determination of VIF resistance is the calculation of the Meyer's index n from the slope of the plot of ln(P)−ln(d). As shown in Table 3, the Mayer's index varied from 1.92 to 2.05, that is, very close to 2. When the Meyer's index n = 2, then there is no Indentation Size Effect (ISE). In order to identify the cracking mode the experimental slopes of the ln(c)−ln(P) and ln(l)−ln(P) plots were compared to 0.66 and 2(1−1/n), respectively.

Glass	GP0	GP1	GP2	GP3	GP4
At.% (Exp.)	0	1.02	2.18	3.32	4.12
Hv (GPa)	4.79 ± 0.04	5.07 ± 0.05	5.38 ± 0.06	5.62 ± 0.05	5.86 ± 0.07
E (GPa)	51 ± 3	63 ± 3	73 ± 4	81 ± 3	90 ± 3
Meyer's index n	1.97	2.03	2.05	1.98	1.92
ln(c)-ln(P) slope	0.661	0.659	0.669	0.672	0.679
ln(l)-ln(P) slope	0.8206	0.8339	0.9175	0.9527	0.9746
K_{ifr} ($MPa.m^{1/2}$)	1.01 ± 0.03	1.06 ± 0.02	1.15 ± 0.02	1.30 ± 0.02	1.42 ± 0.03

Table 3: Hardness (Hv), Young's modulus (E) and VIF resistance (K_{ifr}) results measured by indentation methods for GPx Si-Ca-Na-P-O-N glasses

As an example, for the GP3 glass, the Meyer's index calculated from the slope of the plot of ln(P)−ln(d) is equal to 1.98 and 2(1−1/n) is equal to 0.989. In this particular case, the experimental slopes of the ln(c)−ln(P) and ln(l)−ln(P) plots, shown in Fig. 8, are equal to 0.672 and 0.9527, respectively. Correlation factor for ln(c)−ln(P) is r=0.9896 and, for ln(l)−ln(P), r=0.9682. Comparing the values of the slopes to 0.66 and 0.989, it can be concluded that the cracking mode is Radial Median type. From the results shown in Table 3 for all glasses, it appears that the cracking mode is Radial Median type.

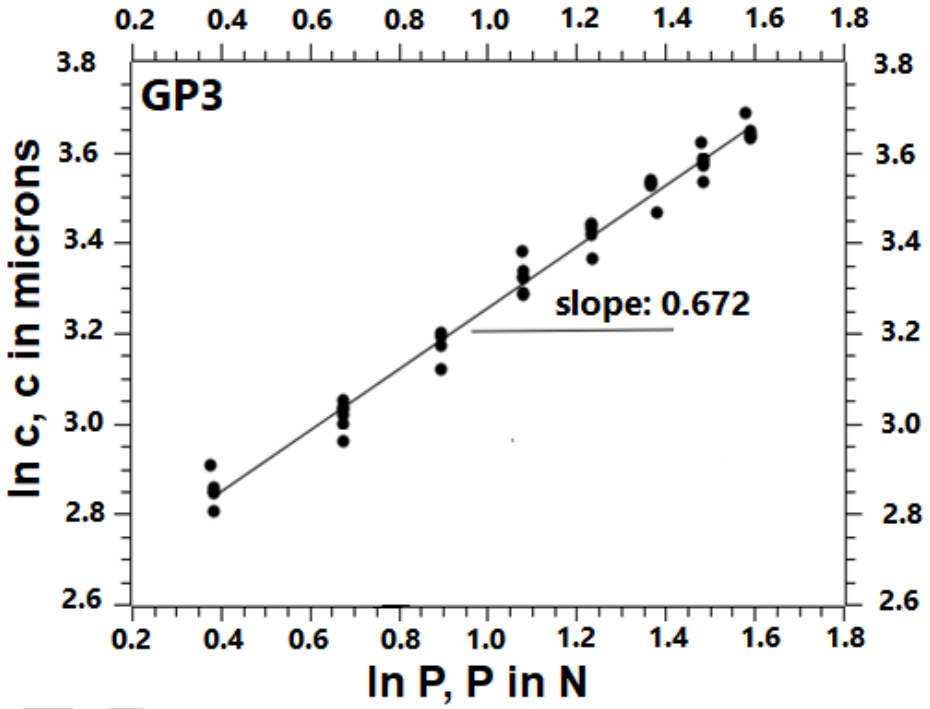

(a)

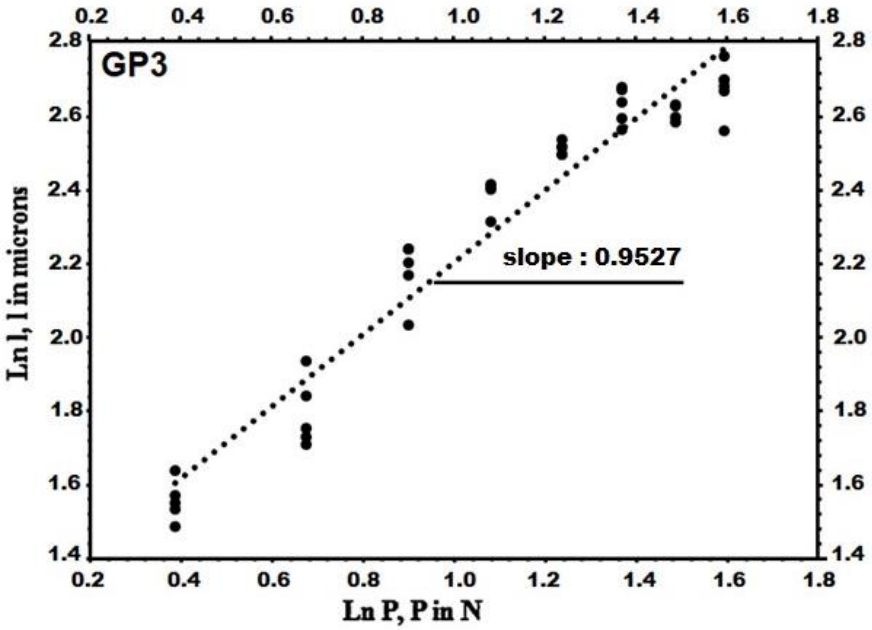

(b)

Fig. 8: Calculation of (a) slope of ln(c)-ln(P) plot, and (b) slope of ln(l)-ln(P) plot for GP3 glass

Fig. 9 shows the variation of the Vickers indentation fracture resistance, K_{ifr}, with analysed nitrogen content for the glasses.

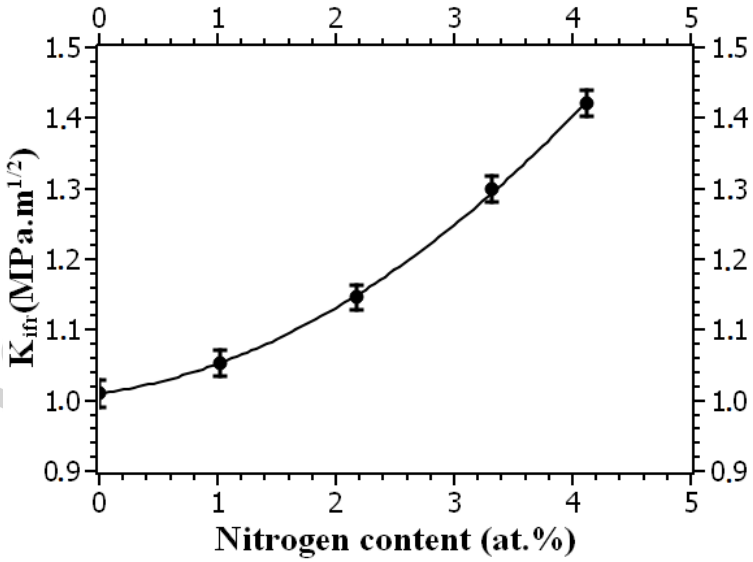

Fig. 9: Vickers indentation fracture resistance (VIF), K_{ifr}, of Na–Ca–P–Si–O–N glasses as a function of nitrogen content

The substitution of nitrogen for oxygen results in an increase in K_{ifr} from 1.01±0.03 MPa.m$^{1/2}$ at 0 at.% N to 1.42±0.03 MPa.m$^{1/2}$ (40% increase) at 4.12 at.% N. The increase in K_{ifr} is non-linear and increases much more as nitrogen substitution increases. For this reason, the experimental results can be modelled by a power law as follows:

$$K_{ifr} = K_{ifr0} + m[\mathrm{N}]^n \quad (11)$$

where K_{ifr0}, m are constants, [N] is N content in at.% and n is the exponent. K_{ifr0} is considered to be the *VIF resistance* of the base glass with 0 at.% N.

Thus the change in K_{ifr} with nitrogen may be given by the following empirical relationship:

$$K_{ifr}(MPa.m^{1/2}) = 1.01 + 0.023[\mathrm{N}] + 0.019[\mathrm{N}]^2 \quad (12)$$

These increases in mechanical properties with nitrogen content indicate that the incorporation of N stiffens the network structure of these glasses. This increase in rigidity of the glass network has been previously explained [12,16] by the extra cross-linking provided by the increasing amount of trivalent N^{3-} ion in place of the divalent O^{2-} ion with formation of SiO_3N and SiO_2N_2 tetrahedra, each of which will have extra bridging anions compared with a SiO_4 unit. This is further explored in the analysis of glass structure by solid state NMR spectroscopy.

3.5. Magic Angle Spinning Nuclear Magnetic Resonance (MAS NMR) Spectroscopy

3.5.1. ^{29}Si MAS NMR

Fig. 10 shows the ^{29}Si MAS NMR spectra of GP0, GP1 and GP3 glasses. On the spectrum of the GP0 glass, the main contributions in the signal are located around −80 and −91 ppm, attributed respectively to Q^2 (35%) units and Q^3 (65%) units [14,34]. Q^2 signifies that the structure consists of SiO_4 tetrahedra linked by 2 bridging oxygens (-Si-O-Si-) per tetrahedra to form chains (and rings) with a significant number of these cross-linked, that is, with 3 bridging oxygens (Q^3). Na and Ca are network modifiers that disrupt the network by forming non-bridging oxygens (NBOs). Introduction of nitrogen into the anionic network produces a wider variety of silicon environments. Three new bands around −105 ppm, −73 ppm and −62 ppm appear, attributed to Q^4 (SiO_4 tetrahedra each with 4 bridging oxygens), [SiO_3N] and [SiO_2N_2] units, respectively [14,23].

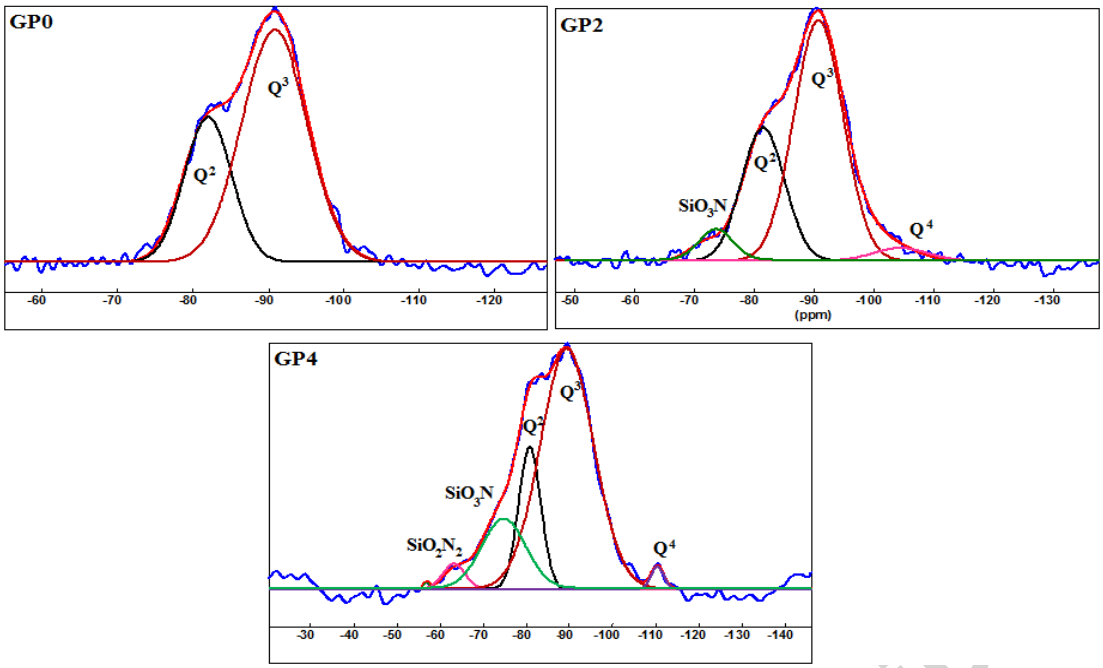

Fig. 10: Deconvolution of ^{29}Si NMR MAS spectra of GPx glasses

The changes in the populations of Q^2, Q^3, Q^4, SiO_3N and SiO_2N_2 units as a function of nitrogen content are given in Fig. 11. When nitrogen is initially introduced, SiO_3N tetrahedra are formed with a reduction in Q^3 units. Further addition of nitrogen results in more SiO_3N tetrahedra, fewer Q^3 units and the appearance of small amounts of Q^4 units and SiO_2N_2 tetrahedra. As N content increases further, small increases are observed in the proportions of SiO_3N tetrahedra, Q^4 units, SiO_2N_2 tetrahedra at the expense of Q^3 units and also Q^2 units at higher nitrogen contents.

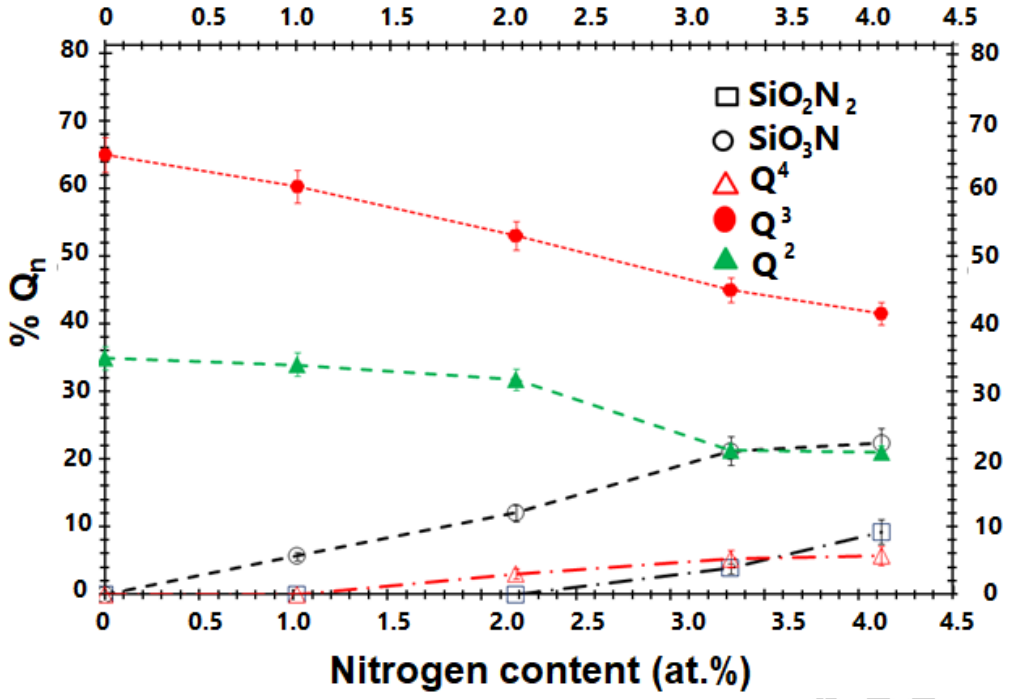

Fig. 11: Effect of nitrogen content on percentages of Q^2, Q^3, Q^4, SiO_3N and SiO_2N_2 for GPx glasses

3.5.2. ^{31}P MAS NMR

Fig. 12 shows the ^{31}P MAS NMR spectra as a function of the nitrogen content of the glasses. All spectra show a single symmetric resonance with chemical shift varying slightly with N content from ~10.0 (±0.5) ppm for the GP0 glass, ~10.2 (±0.5) ppm for the GP1 glass to ~9.5 (±0.5) ppm for the GP4 glass. Indeed, this is not significant as the shift is of the same order of magnitude as the uncertainty.

Previous results on soda-lime-phosphosilicate glasses [35] have attributed single resonances with similar chemical shifts to a mixed sodium and calcium orthophosphate (Q^0) complex without P entering the silicate glass network. Charge balance is by Na^+ and/or Ca^{2+} ions. Phosphorus is therefore isolated from the silicate network and removes Na^+ and Ca^{2+} cations from their network-modifying role. The increase in the amount of nitrogen does not affect the spectra so N has no influence on the chemical environment of phosphorus and therefore it is always associated with the silica network and not the phosphate network.

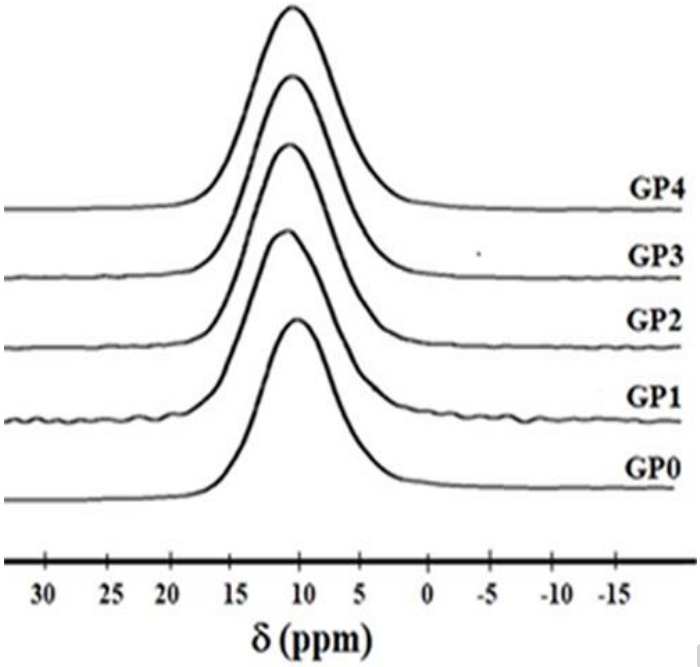

Fig. 12: ^{31}P MAS-NMR spectra of GPx glasses

3.6. Bioactivity tests

The XRD patterns for GP0, GP2 and GP4 glasses after 15 days of immersion in the SBF are presented in Figure 13. The formation of apatite is confirmed by the three strongest XRD peaks appearing at $2\theta = 26.30^{o}$, 32.27^{o} and 53.15^{o} that correspond, respectively, to (002), (112) and (004) planes. However, the intensities of these major peaks decrease with nitrogen content showing that the crystallinity of this layer decreases with N content, suggesting that nitrogen may slow the crystallization of the apatite layer and therefore may inhibit bioactivity.

The mechanism of hydroxyapatite deposition on the surface of Na_2O-CaO-SiO_2 glasses in simulated body fluid has been reported by Ohtsuki et al. [36]. When these materials are exposed to SBF for a period of time, soluble ionic species (Na, Ca and Si ions) are released and a high surface area hydrated silica and polycrystalline hydroxyl-carbonate apatite (HCA) bi-layer is formed on the glass surface.

The SEM micrographs of the bioactive glasses immersed for 15 days in the SBF are presented in Figure 14 which shows that, on the oxide glass GP0 and the N-doped glass GP4, a hydroxyapatite layer is formed. These may be compared with the SEM micrographs of GP0 and GP4 glass surfaces before soaking in SBF in Figure 2.

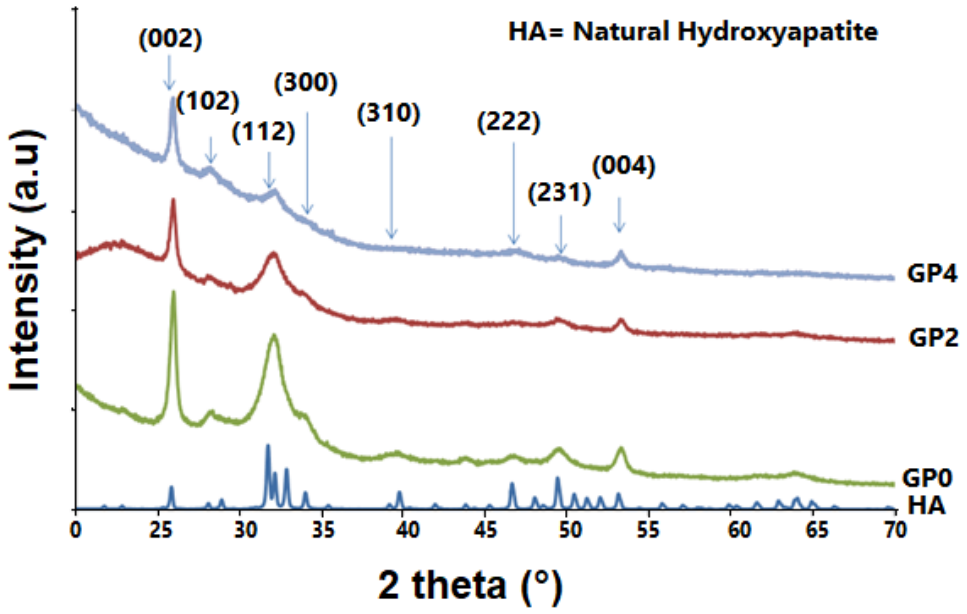

Fig. 13: X-ray diffraction patterns of GPx bioactive glasses after soaking in SBF solution for 15 days

The morphologies and sizes of the HA crystals vary with the content of nitrogen. Indeed, as shown in Figure 14a for glass GP0, a significant amount of a homogeneous hydroxyapatite layer is deposited on the surface as confirmed by X-ray diffraction (see Fig. 13). Released calcium ions supersaturate the SBF solution and react with phosphate ions in the vicinity of the surface allowing apatite nuclei to form. The orthophosphate phase in the glass would be more soluble than the silicate phase and leads to phosphorus super-saturation of SBF. This would result in an increase of the rate of apatite deposition on the glass surface.

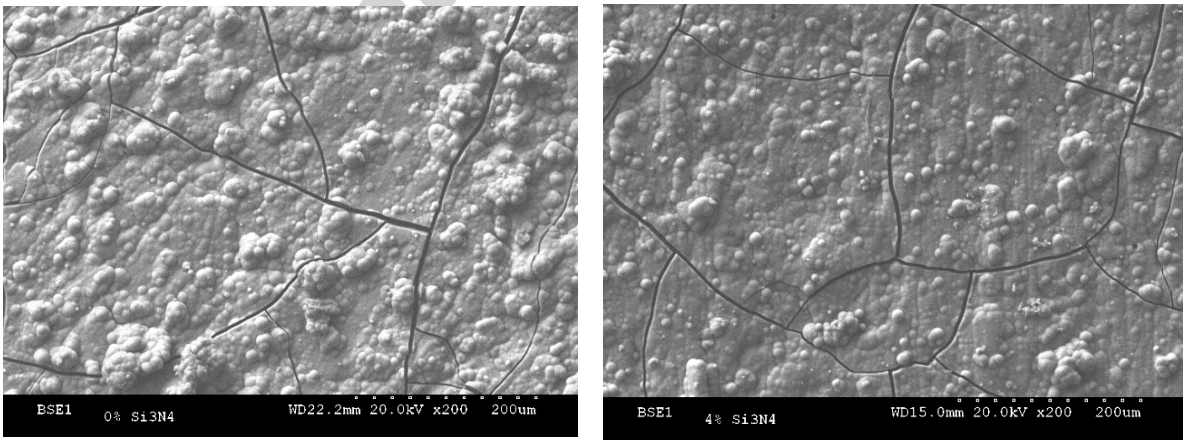

a) **b)**

Fig. 14: SEM micrographs of: a) glass GP0 and b) glass GP4 surfaces after soaking in SBF

When nitrogen content increases, the hydrated silica (silanol) acts as heterogeneous nucleation sites for crystallisation of apatite and hence solubility of the silicate network is important for the kinetics of these reactions. A higher level of crystallization of HA is observed for glasses with lower nitrogen contents compared with GP4. The increasing cross-linking of the silicate network with increasing N content results in a less soluble bioactive glass and, hence, reduced bioactivity.

As shown in Figure 14b for glass GP4, the HA layer is more heterogeneous and the size of the crystals are smaller. This micrograph confirms the XRD results showing the retardation of the hydroxyapatite crystal growth at the highest N content. Previous work on oxynitride glasses without P_2O_5 has shown that optimising the N content allows tailoring of different levels of bioactivity for these glasses [22].

3.7. Cytotoxicity tests

Figure 15 shows the results of viability tests, performed on the GPx glasses and nickel powder as a function of powder concentration. The viability percentage is determined by the ratio between the number of surviving L132 cells in the medium exposed to the powder sample and the number of surviving cells in a control medium. LC 50 corresponds to the death of 50% of the cells. The number of introduced cells is the same in all the samples and the control.

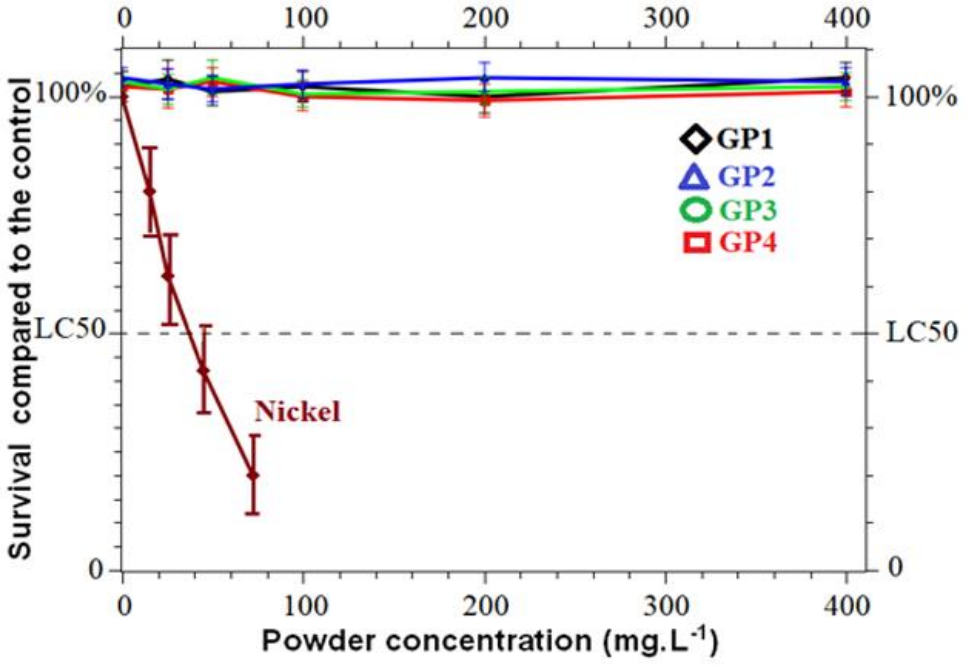

Fig. 15: L132 viability tests on GPx glasses and nickel

It is necessary to compare with the control because the survival ratio is never really 100%. Indeed, the cells are stressed during the subculture which leads to the death of a small fraction.

A material is considered cytotoxic if its addition into the culture medium increases the cell death as the powder concentration increases. In the present case, these bioactive GPx glasses do not show this behavior. With a concentration of 400 mg L^{-1}, the average survival of L132 cells is 100% for all GPx glasses. Thus, none of the glasses is cytotoxic. It is interesting to note that these bioactive glasses containing P and N appear to show a higher survival ratio than 100% at low concentrations (112% for GP0 and 105% for GP4 with 25 ml L^{-1}). This would indicate that these glasses improve growth conditions for the L132 cells.

4. Conclusions

Glasses with molar composition: $29Na_2O–13.5CaO–2.5P_2O_5–(55−3x)SiO_2–xSi_3N_4$ (x = 1, 2, 3, 4 is the no. of moles of Si_3N_4) have been synthesised and characterised. The following conclusions can be made:

(1) The experimental strategy of using different steps for addition of P and N proved to be successful in terms of minimising weight losses. Elemental analysis confirmed that much lower amounts of N and P were lost from each composition than expected from previous reports. Thus homogeneous Na-Ca-Si-O-P-N glasses were formed with up to 1.5 at.% P and 4.1 at.% N. The overall importance of this work is that while phosphate glasses containing N are well known, to our knowledge this is the first report of successfully prepared glasses containing P and N with such high SiO_2 content.

(2) Density increases by 1.6% when 4.12 at.% N is substituted for oxygen which is a result of the higher compactness of the glass network and lower molar volume.

(3) The substitution of 4.12 at.% N for oxygen results in linear increases in glass transition temperature (6%), hardness (18%) and elastic modulus (74%). These trends indicate that the incorporation of nitrogen, which is tri-coordinated with silicon compared with 2-fold coordination for oxygen, results in extra cross-linking and stiffening of the glass network.

(4) The substitution of 4.12 at.% N for oxygen results in an increase in Vickers Indentation Fracture (VIF) resistance (K_{ifr}) of 40% according to a power law relationship.

(5) The characterization of these Na-Ca-Si-P-O-N glasses using ^{29}Si MAS-NMR has shown that the increase in connectivity of the glass network can be explained by the formation of an increasing number of Q^4, SiO_3N and SiO_2N_2 units with nitrogen content, thus forming extra bridging anions at the expense of Q^3 and Q^2 units. From ^{31}P MAS-NMR analysis, phosphorus is present as a mixed sodium and calcium orthophosphate (Q^0) complex. The presence of nitrogen does not affect the chemical environment of phosphorus.

(6) Following immersion of the glasses in SBF for 15 days, a homogeneous layer of hydroxyapatite was formed on the surfaces of the Na-Ca-Si-P-O-N glasses. The crystallinity of this layer decreases with N content suggesting that N may inhibit bioactivity. The extra cross-linking of the network with N leads to a less soluble glass in SBF. Optimisation of the N content would allow tailoring of different levels of bioactivity.

(7) The cytotoxicity tests show that the Na-Ca-Si-P-O-N glasses are not cytotoxic and, at low powder concentrations, exhibit even higher survival ratios than 100%, indicating improvements in growth conditions for the cells.

Funding

This research did not receive any specific grant from funding agencies in the public, commercial, or not-for-profit sectors.

References

[1] L.L. Hench, 1991, "Bioceramics: From Concept to Clinic," *J. Am. Ceram. Soc.*, 74 (7), 1487-1510.
[2] L. L. Hench, 2006, "The story of Bioglass," *J. Mater. Sci. – Mater. Med.*, 17, 967-978.
[3] T. Kokubo, 1990, "Surface chemistry of bioactive glass-ceramics," *J. Non-Cryst. Sol.*, 120, pp. 138-151.
[4] L.L. Hench, R.J. Splinter, W.C. Allen, T.K. Greenlee Jr., 1971, "Bonding Mechanisms at the Interface of Ceramic Prosthetic Materials," *J. Biomed. Mater. Res.*, 2(1), 117-141.

[5] C.Y. Kim, A.E. Clark, L.L. Hench, 1989, "Early Stages of Calcium-Phosphate Layer Formation in Bioglass," *J. Non-Cryst. Sol.*, 113(2-3), 195-202.

[6] J.R. Jones, 2013, "Review of bioactive glass: From Hench to hybrids," *Acta Biomater.* 9, 4457-4486.

[7] H. Kim, F. Miyaji, T. Kokubo, C. Ohtsuki, T. Nakamura, 1995, "Bioactivity of Na_2O–CaO–SiO_2 glasses," *J. Am. Ceram. Soc.*, 78 (9), 2405-2411.

[8] P. Ducheyne, L.L. Hench, A. Kagan, and M. Martens, 1979, "Short-Term Bonding Behaviour of Bioglass Coatings on Metallic Substrate," *Arch. Orthop. Traumat. Surg.*, 94, 155-160.

[9] H. Oonishi, L.L. Hench, J. Wilson, F. Sugihara, E. Tsuji, M. Matsuura, 2000, "Quantitative comparison of bone growth behavior in granules of Bioglass®, A-W glass-ceramic, and hydroxyapatite," *J. Biomed. Mater. Res.*, 51, 37-46.

[10] L.L. Hench, 2011, "Bioactive materials for gene control," In: L.L. Hench, J.R. Jones, M.B. Fenn, eds. *New materials and technologies for healthcare*. Singapore: World Scientific, pp. 25–48.

[11] K.R. Rust, G.T. Singleton, J. Wilson, P.J. Antonelli, 1996, "Bioglass middle ear prosthesis: long-term results," *Am. J. Otolaryngol.*, 17, 371-374.

[12] S. Hampshire, 2008, "Oxynitride glasses," *J. Euro. Ceram. Soc.*, 28, 1475-1483.

[13] S. Hampshire, R.A.L. Drew, and K.H. Jack, 1984, "Viscosities, Glass Transition Temperatures, and Microhardness of Y-Si-A1-O-N Glasses," *J. Am. Ceram. Soc.*, 67, C46-47.

[14] A. Bachar, C. Mercier, A. Tricoteaux, A. Leriche, C. Follet, M. Saadi, and S. Hampshire, 2012, "Effects of addition of nitrogen on bioglass properties and structure," *J. Non-Cryst. Sol.*, 358, 693-701.

[15] A.R. Hanifi, A. Genson, M.J. Pomeroy, S. Hampshire, 2012, "Independent but Additive Effects of Fluorine and Nitrogen Substitution on Properties of a Calcium Aluminosilicate Glass," *J. Am. Ceram. Soc.*, 95(2), 600-606.

[16] P.F. Becher, S. Hampshire, M.J. Pomeroy, M.J. Hoffmann, M.J. Lance, and R.L. Satet, 2011, "An Overview of the Structure-Property Relationships in Silicon-Based Oxynitride Glasses," *Int. J. Appl. Glass Sci.*, 2(1), 63-83.

[17] A. Bachar, C. Mercier, C. Follet, N. Bost, F. Bentiss, S. Hampshire, 2016, "An Introduction of the fluorine and nitrogen on properties of Ca-Si-Al-O glasses," *J. Mater. Environ. Sci.*, 7, 347-355.

[18] A. Bachar, A. Tricoteaux, A. Leriche, C. Follet, S. Hampshire, M. Towler, 2015, "Effect of Nitrogen on Properties of Na_2O–CaO–SrO–ZnO–SiO_2 Glasses," *J. Am. Ceram. Soc.*, 98(3), 748-757.

[19] M.J. Pomeroy, E. Nestor, R. Ramesh, S. Hampshire, 2005, "Properties and crystallisation of rare earth SiAlON glasses containing mixed trivalent modifiers," *J. Am. Ceram. Soc.*, 88, 875-881.

[20] A. Kidari, M.J. Pomeroy, S. Hampshire, 2012, "Novel Na–Li–SiAlPON glasses prepared by melt synthesis using AlN," *J. Euro. Ceram. Soc.*, 32, 1389-1394.

[21] C. Duée, F. Désanglois, I. Lebecq, G. Moreau, A. Leriche, C. Follet-Houttemane, 2009, "Mixture designs applied to glass bioactivity evaluation in the Si–Ca–Na system," *J. Non-Cryst. Sol.*, 355, 943–950.

[22] Ahmed Bachar, Cyrille Mercier, Arnaud Tricoteaux, Anne Leriche, Claudine Follet, Stuart Hampshire, 2016, "Bioactive Oxynitride Glasses: Synthesis, Structure and Properties," *J. Euro. Ceram. Soc.*, 36 (12), 2869-2881.

[23] A. Bachar, C. Mercier, A. Tricoteaux, S. Hampshire, A. Leriche, and C. Follet, 2013, "Effect of nitrogen and fluorine on mechanical properties and bioactivity in two series of bioactive glasses," *J. Mech. Behavior Biomed. Mater.*, 23, 133-148.

[24] A.G. Evans and E.A. Charles, 1976, "Fracture Toughness Determinations by Indentation," *J. Am. Ceram. Soc.,* 59, 371-372.

[25] G.D. Quinn, R.C. Bradt, 2007, "On the Vickers indentation fracture toughness test," *J. Am. Ceram. Soc.*, 90, 673-680.

[26] H. Miyazaki, Y.-i. Yoshizawa, K. Hirao, and T. Ohji, 2010, "Indentation fracture resistance test round robin on silicon nitride ceramics," *Ceram. Int.,* 36, 899-907.

[27] S. Dériano, A. Jarry, T. Rouxel, J.C. Sangleboeuf, and S. Hampshire, 2004, "The indentation fracture toughness (Kc) and its parameters: the case of silica-rich glasses," *J. Non-Cryst. Sol.*, 344, 44-50.

[28] C.B. Ponton, D.R. Rawlings, 1989, "Vickers indentation fracture toughness test. Part 1. Review of literature and formulation of standardized indentation toughness equations," *Mater. Sci. & Tech.,* 5(9), 865-872.

[29] D. Chicot, A. Tricoteaux, 2010, "Chapter 7: Mechanical properties of ceramics by indentation: Principle and applications," In: W. Wunderlich (ed.) *Ceramic Materials*, InTech University Campus STeP Ri, Rijeka, Croatia, pp. 115–154.

[30] E. Meyer, 1908, "Untersuchen über härteprüfung und Härte," Z. Ver. deutscher Ing., 52, 645-654.

[31] M.E. Frazier, T.K. Andrews, In: N. Kharash, (Ed.) 1979, "In vitro clonal growth assay for evaluating toxicity of metal salts," *Trace Metals in Health and Disease*, Raven Press, New York. pp. 71-81.

[32] J.C. Hornez, A. Lefèvre, D. Joly, and H.F. Hildebrand, 2002, "Multiple parameter cytotoxicity index on dental alloys and pure metals," *Biomolec. Eng.,* 19, 103-117.

[33] M.J. Pomeroy and S. Hampshire, 2008, "SiAlON glasses: effects of nitrogen on structure and properties," *J. Ceram. Soc. Jpn.,* 116, 755-761.

[34] C. Mercier, C. Follet-Houttemane, A. Pardini, and B. Revel, 2011, "Influence of P_2O_5 content on the structure of SiO_2-Na_2O-CaO-P_2O_5 bioglasses by ^{29}Si and ^{31}P MAS-NMR," *J. Non-Cryst. Sol.,* 357, 3901-3909.

[35] M.D. O'Donnell, S.J. Watts, R.V. Law, R.G. Hill, 2008, "Effect of P_2O_5 content in two series of soda lime phosphosilicate glasses on structure and properties – Part I: NMR," *J. Non-Cryst. Sol.*, 354, 3554-3560.

[36] C. Ohtsuki, T. Kokubo and T. Yamamuro, 1992, "Mechanism of apatite formation on CaO- SiO_2-P_2O_5 glasses in a simulated body fluid," *J. Non-Cryst. Sol.,* 143, 84-92.